Available online at www.sciencedirect.com

ScienceDirect

Geochimica et Cosmochimica Acta 189 (2016) 377–390

Geochimica et Cosmochimica Acta

www.elsevier.com/locate/gca

The valence and coordination of titanium in ordinary and enstatite chondrites

Steven B. Simon [a,*], Stephen R. Sutton [a,b], Lawrence Grossman [a,c]

[a] Dept. of the Geophysical Sciences, 5734 S. Ellis Ave, The University of Chicago, Chicago, IL 60637, United States
[b] Center for Advanced Radiation Sources (CARS), 5640 S. Ellis Ave, The University of Chicago, Chicago, IL 60637, United States
[c] The Enrico Fermi Institute, 5640 S. Ellis Ave, The University of Chicago, Chicago, IL 60637, United States

Received 3 February 2016; accepted in revised form 9 June 2016; Available online 17 June 2016

Abstract

One way to better understand processes related to chondrite metamorphism is to evaluate changes in chondrite features as a function of petrologic type. Toward this end the valence and coordination of Ti in olivine and pyroxene in suites of ordinary (H, L, and LL) and enstatite (EH and EL) chondrites of types 3 through 6 have been determined with XANES spectroscopy. Trivalent Ti, typically 10–40% of the Ti in the analytical volumes, was found in ordinary chondrites of all types, despite the stability of oxidized iron in the samples. Average valences and the proportions of Ti that are in tetrahedral coordination generally decrease with increasing grade between types 3.0 and 3.5, increase from 3.5 to 4, and then level off. These trends are consistent with previous studies of chondrite oxidation states using other methods, except here the onset of oxidation is observed at a lower type, ~3.5, than previously indicated (4). These results are also consistent with previous suggestions that oxidation of higher-grade ordinary chondrite samples involved exposure to aqueous fluids from melting of accreted ice. In the enstatite chondrites, typically 20–90% of the Ti is trivalent Ti, so it is reduced compared to Ti in the ordinary chondrites. Valence decreases slightly from petrologic type 3 to 4 and increases from 4 to 6, but no increases in tetrahedral coordination with petrologic type are observed, indicating a redox environment or process distinct from that of ordinary chondrite metamorphism. The presence of Ti^{4+} in the E chondrites supports previous suggestions that they formed from oxidized precursors that underwent reduction. Unlike ordinary chondrites, enstatite chondrites are thought to have been derived from a body or bodies that did not accrete ice, which could account for their different valence-coordination-petrologic type relationships. The hypothesis, based on observations of unmetamorphosed chondrules and supported by laboratory experiments, that equilibration of Ti valence is sluggish compared to that of Fe could account for the coexistence of reduced Ti and oxidized Fe seen in chondrites of all petrologic types.

Keywords: Ordinary chondrites; Enstatite chondrites; Ti valence; Chondrite metamorphism

1. INTRODUCTION

The ordinary (the H, L, and LL groups) and enstatite (E) chondrites have undergone varied extents of thermal metamorphism, from very low-grade (type 3), with little modification of textures and mineral compositions, to high-grade (type 6), with homogenization of Fe/Mg ratios of ferromagnesian silicates and extensive recrystallization (Van Schmus and Wood, 1967). Knowledge of the conditions to which these materials were subjected and their responses to them is necessary for a sound understanding of the evolution of their parent bodies, and early planetary processes in general. Thus, there is much interest in constraining the temperature ranges of the different grades,

* Corresponding author.
E-mail address: sbs8@uchicago.edu (S.B. Simon).

http://dx.doi.org/10.1016/j.gca.2016.06.013
0016-7037/

their cooling rates, and redox environments. While a good picture of the thermal histories of chondrites has been obtained, relatively little work has focused on redox reactions during metamorphism. Oxidation during metamorphism from type 4 to 6 has been inferred by McSween and Labotka (1993), Gastineau-Lyons et al. (2002) and by Dunn et al. (2010). McSween and Labotka (1993) noted that, in ordinary chondrites with increasing metamorphic grade of a given chemical meteorite type, FeO/MgO ratios in olivine and pyroxene increase; olivine/pyroxene ratios increase; and metal contents decrease. These features were interpreted by McSween and Labotka (1993) as consistent with oxidation. These authors further suggested that the oxidizing agent was an aqueous fluid derived by melting of ice present on the parent bodies, and that sufficient carbon was present in the original assemblages that initial stages of chondrite metamorphism were reducing until temperatures at which graphite would dissolve into metal were reached. A study by Menzies et al. (2005), using Mössbauer spectroscopy and X-ray diffraction, showed that unequilibrated ordinary chondrites of types 3 to 4 become more reduced with increasing grade, and they noted that bulk carbon contents decrease as well, from 0.02 to 0.04 wt% in type 3.0 samples to zero in type 4 samples.

From these studies, what appears most likely is that reduction occurred during metamorphism from type 3 through 4 and oxidation from 4 through 6. A study by Kessel et al. (2007), in which the equilibration temperatures and fO_2s of a suite of H chondrites were determined based on textures, phase compositions and calculated olivine-spinel equilibration temperatures, however, found no systematic variation of fO_2 with metamorphic grade. Thus, the effects of planetary metamorphism on the redox state of ordinary chondrites are not completely understood.

Enstatite chondrites, whether equilibrated or unequilibrated, are dominated by reduced assemblages of FeO-poor silicates, Si-bearing metal, and sulfides, though FeO-bearing silicates can be found in unequilibrated enstatite chondrites (Lusby et al., 1987; Weisberg et al., 1994). In contrast to the fluid-assisted planetary metamorphism inferred for the ordinary chondrites, many equilibrated (types 4–6) enstatite chondrites exhibit petrographic and geochemical features that are consistent with impact heating and melting (Rubin and Wasson, 2011). These are highly reduced, metal-rich materials, with euhedral enstatite, graphite and sinoite. Rubin and Wasson (2011) suggested that, during melting, Si originally present in metal could have reacted with FeO in the primary, unequilibrated material, forming silica plus metallic Fe.

Thus, it seems likely that enstatite chondrites initially contained oxidized components and were metamorphosed under reducing conditions, whereas for ordinary chondrites the situation is more complex, with reduction of Fe in the presence of carbon at low grades and indications that oxidation followed at higher grades, although there is no clear record of an increase in fO_2.

With the exception of the Mössbauer spectroscopic study by Menzies et al. (2005), most of what we know about the effects of metamorphism on the redox state of chondrites is based on interpretation of observations of features, such as pyroxene/olivine ratios, that are possibly related to redox processes, rather than direct measurements. In an attempt to improve our understanding of the redox environment during, and the effects of, chondrite metamorphism, we have measured the valence and coordination of Ti in pyroxene and olivine *in situ* in suites of H, L, and LL ordinary chondrites and EH and EL enstatite chondrites of petrologic types 3 through 6. The valence of Ti is of interest because chondrules and/or their precursors formed under such reducing conditions that Ti^{3+} was stabilized in addition to Ti^{4+}. In primary phases in chondrites, Fe is either divalent (in silicates and oxides) or metallic. Other elements of possible variable valence in chondrites are V and Cr. The former is in very low abundance in the samples considered here, and the latter will be investigated in a future study. The samples included in the study are listed in Table 1. As the Table shows, there are subdivisions between types 3 and 4 for low-grade meteorites, but there are no subdivisions between 4 and 5 or between 5 and 6. Preliminary results of this work were reported by (Simon et al. 2012, 2013, 2015).

2. ANALYTICAL METHODS

Thin sections were examined optically and with a JEOL JSM-5800 LV scanning electron microscope. In each sample, a suite of chondrules (or, in chondrule-free grade 6 samples, typical, recrystallized areas) was selected for analysis. Most of the chondrules analyzed are porphyritic, as barred and radial chondrules tend to be too fine-grained for the μm-scale spatial resolution of the XANES instrument used here. Quantitative wavelength-dispersive analyses of phases in the selected chondrules and areas, including XANES analysis spots, were obtained with a fully automated Cameca SX-50 electron microprobe operated at 15 kV. Data were reduced using the modified ZAF correction procedure PAP (Pouchou and Pichoir, 1984).

The valence and coordination of Ti were determined quantitatively by X-ray absorption near-edge structure (XANES) spectroscopy using the undulator-based microprobe at Sector 13 (GeoSoilEnviroCARS) at the Advanced Photon Source, Argonne National Laboratory (Sutton and Rivers, 1999; Sutton et al., 2002; Sutton and Newville, 2014). This technique is based on the intensity and energy of the pre-edge absorption peak, which vary systematically as a function of valence and coordination environment. The three possible valence-coordination combinations: octahedral Ti^{3+}; octahedral Ti^{4+}; and tetrahedral Ti^{4+} yield pre-edge peaks with characteristic energy-intensity combinations. Results for unknowns are derived from mixing lines between endmember spectra. Valences are reported as values between 3 and 4, which represent the average valences of the analytical volumes. Orientation effects can cause spurious Ti valence determinations, especially in samples with significant tetrahedral Ti components. Analysis of multiple grains of a phase within a sample and use of merged spectra can mitigate this effect if the grains are randomly oriented, which is assumed to be the case for the porphyritic chondrules. Analytical conditions and methods are as described by Simon et al. (2007), except that upgrades to the facility

Table 1
Petrologic types of all samples and chondrules, and, where applicable, numbers of each chondrule type analyzed.

Meteorites		Chondrules					
Sample	Pet. Type	Type IA	Type IB	Type IAB	Type IIA	Type IIB	Type IIAB
H chondrites							
A-881026,61-2	3.0		1	2	3	1	1
Sharps	3.4	1	1	1		1	1
Dhajala	3.8				3		3
Weston	4	2			1		4
Lost City	5					2	4
Guareña	6						
L chondrites							
LEW 86158,4	3.2		1	1	1		
LEW 86505,8	3.4			1	1		2
ALHA 81025,12	3.6			1	1		
ALH 84086,5	3.8			1	1	1	
EET 87557,10	4						2
Park Forest	5				4		2
New Concord	6						
LL chondrites							
Semarkona	3.0			2	1		1
Bishunpur	3.15	1	1	1	1	1	1
Chainpur	3.4	1		1	1		2
Parnallee	3.6	1	1	1	1	1	
LAR 06674,4	3.8		1	1		1	1
Hamlet	4		1	1	1	1	1
Olivenza	5				1	1	1
St. Severin	6						
EH chondrites							
Qingzhen	3*		4			1	
Indarch	4		3				
St. Mark's	5		4				
Y-980211,51-1	6						
EL chondrites							
PCA 91020,15	3		3				
MAC 02747,20	4		3				
TIL 91714,8	5		3				
Hvittis	6						

* Although officially classified as a type 3, the petrologic type of Qingzhen has also been reported as >3.5 (Huss and Lewis, 1995) and 3.6–3.7 (Quirico et al., 2011). Sources of named samples and their specific numbers (if available): U.S. National Museum: Sharps, 6402; Dhajala, 5832-1; Weston, 1180-3; Lost City, 4848-3; Guarena, 1469-3; Semarkona 1805-18; Bishunpur 2359-1; Chainpur, 1251-16; Hamlet, 3455-3; Olivenza, 5955-1; Indarch, 3482-4; St. Mark's, 3027-2. Field Museum of Natural History: Parnallee, 11; New Concord; St. Severin; Hvittis. Univ. of New Mexico: Qingzhen, 636. Antarctic meteorite sources: National Institute of Polar Research: A-881026,61-2 and Y-980211,51-1. All other Antarctic (numbered) samples are from the Antarctic Search for Meteorites (ANSMET) collection.

have allowed reduction of the diameter of the X-ray beam to ~1 μm. Natural and synthetic standards were used for the electron probe work and the XANES analysis.

3. RESULTS

3.1. Sample petrography and mineral chemistry

In unequilibrated (petrologic types 3.0–3.9) ordinary chondrites, olivine and pyroxene exhibit wide ranges of Fe/Mg ratios. Grains may be zoned, and both magnesian (type I) chondrules, in which olivine and pyroxene have <10 mol% fayalite (Fa) and ferrosilite (Fs), respectively, and ferroan (type II) chondrules can be found. In equilibrated ordinary chondrites (petrologic types ⩾4) most ferromagnesian silicates are unzoned in Fe/Mg and almost all chondrules are classified as type II based on their observed Fe/Mg ratios (type I chondrules can be found in some type 4 samples, but they are rare). Type A chondrules are dominated by olivine, type B by pyroxene, and type AB chondrules have both phases but neither is dominant. In enstatite chondrites, both olivine and FeO-bearing pyroxene are rare, and are found only in unequilibrated samples. For a review of chondrite and chondrule mineralogy, see Brearley and Jones (1998). The petrographic types of the chondrules analyzed for this study and the number of each are given in Table 1.

3.1.1. H chondrites

The H chondrite suite considered here consists of one find (Auska-881026, H3.0) and five falls: Sharps (3.4); Dhajala (3.8); Weston (4); Lost City (5); and Guareña (6).

Backscattered electron images of an analyzed chondrule from each of these samples, in order of increasing metamorphic grade, are shown in Fig. 1. Note increasing homogeneity of the electron albedos of individual olivine and pyroxene grains with increasing petrologic type, reflecting increasing homogeneity of Fe/Mg ratios. A total of 37 chondrules (4–8 per H chondrite) were analyzed. All are porphyritic, with various amounts of mesostasis, except for one cryptocrystalline, one compound, and two barred chondrules. The range of olivine compositions is $Fa_{0–23}$, and the pyroxene range is $Fs_{2–23}$. Typical Ti contents, determined by electron probe, range from below detection to 0.25 wt% Ti as TiO_2 in olivine and from below detection to 0.15 wt% in pyroxene.

3.1.2. L chondrites

The sample suite consists of five (Antarctic) finds and the Park Forest (L5) and New Concord (L6) falls. Olivine and/or low-Ca pyroxene was analyzed in two to six chondrules in the petrologic types 3 through 5 samples (Table 1). In addition, grains in two areas in New Concord (L6) were analyzed by XANES. The composition range of olivine in the highly unequilibrated samples (types 3.2–3.8) is $Fa_{1–31}$; in EET 87557 (L4) it is $Fa_{17–29}$; and in the equilibrated samples it is $Fa_{24–25}$. Pyroxene ferrosilite contents are 1–21 mol% in the highly unequilibrated samples, 8–16% in EET 87557, and 20–21% in the equilibrated samples. Typical Ti contents are 0.02–0.06 wt% Ti as TiO_2 in olivine and 0.02–0.20 wt% in pyroxene.

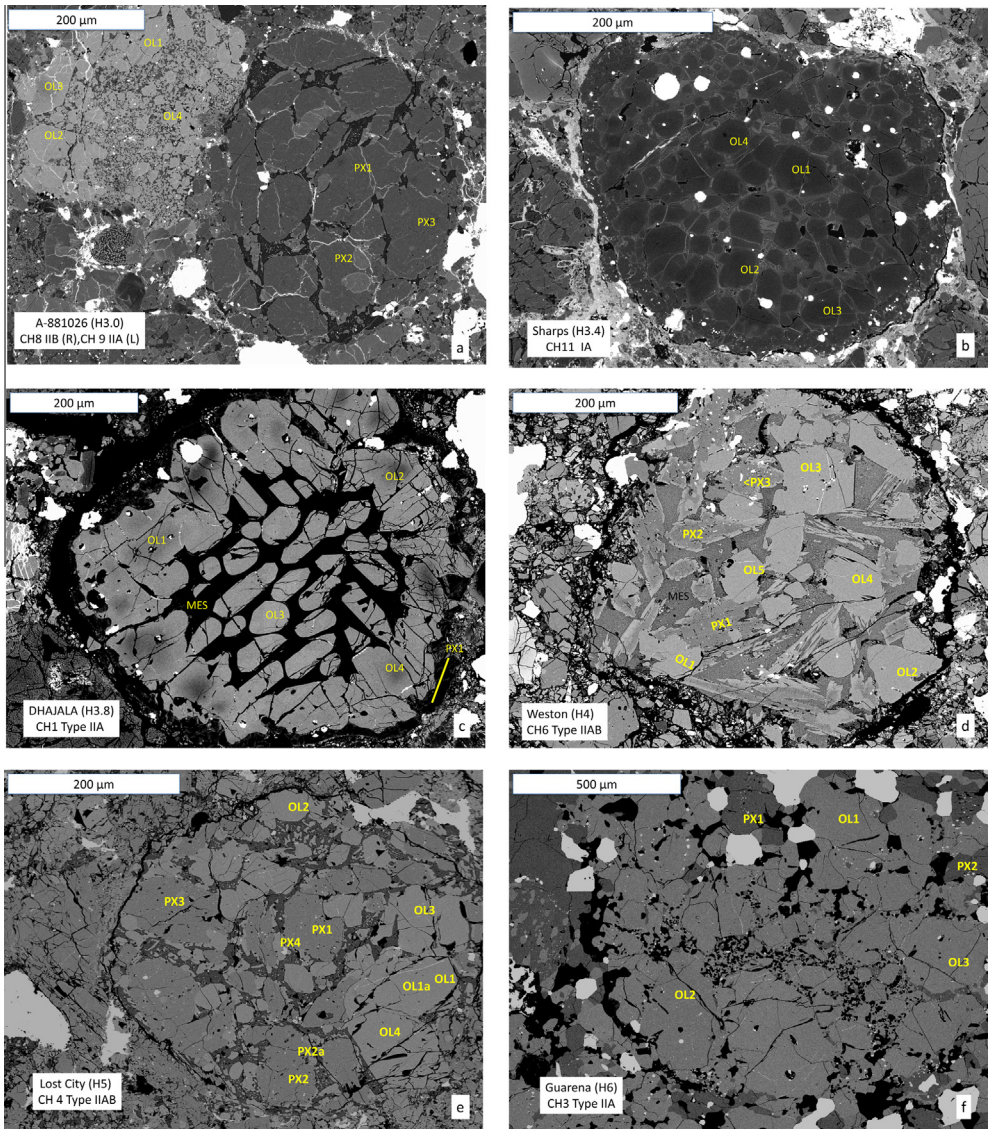

Fig. 1. Backscattered electron (BSE) images of representative chondrules from the H chondrites considered in this study. (a) Two chondrules in A-881026 (H3.0), a type IIA (left) and a IIB (right). (b) A porphyritic type IA chondrule in Sharps (H3.4). (c) A barred type IIA chondrule in Dhajala (H3.8). (d) A porphyritic type IIAB chondrule in Weston (H4). (e) A porphyritic type IIAB chondrule in Lost City (H5). (f) A porphyritic chondrule remnant in Guareña (H6). Yellow labels indicate locations of XANES analyses. OL: olivine; PX: pyroxene; MES: mesostasis. (For interpretation of the references to color in this figure legend, the reader is referred to the web version of this article.)

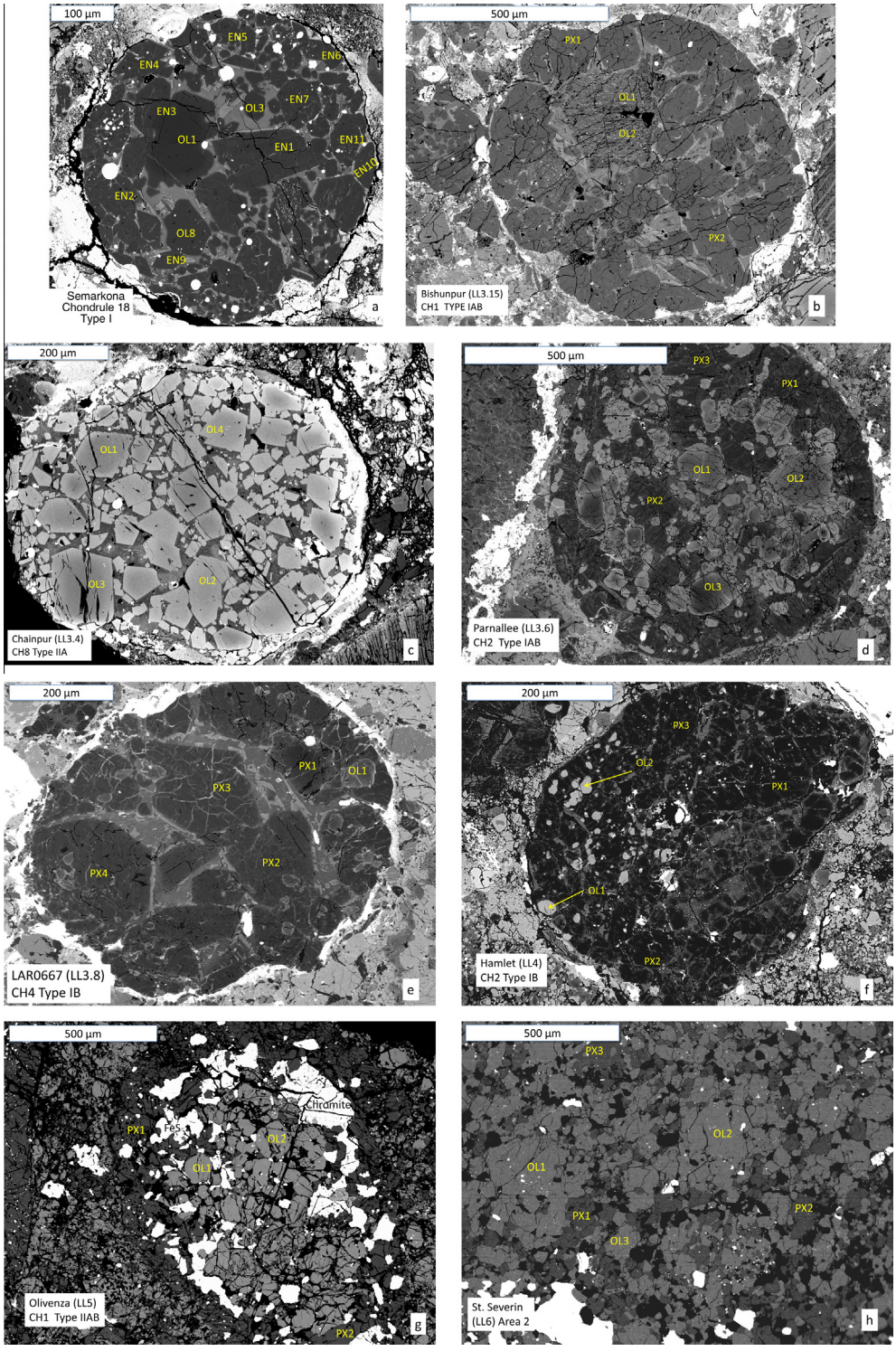

Fig. 2. Backscattered electron images of analyzed chondrules in LL chondrites. (a) A porphyritic type IAB in Semarkona (LL3.0). (b) A porphyritic type IAB in Bishunpur (LL3.15). Note "dusty" olivine grains. (c) A porphyritic type IIA chondrule in Chainpur (LL3.4). (d) A porphyritic type IAB chondrule in Parnallee (LL3.6). (e) A coarse-grained porphyritic type IB chondrule in LAR 0667 (LL3.8). (f) A type IB chondrule in Hamlet (LL4). (g) A type IIAB chondrule in Olivenza (LL5). (h) A representative area in St. Severin (LL6). EN: enstatite; other abbreviations as in Fig. 1.

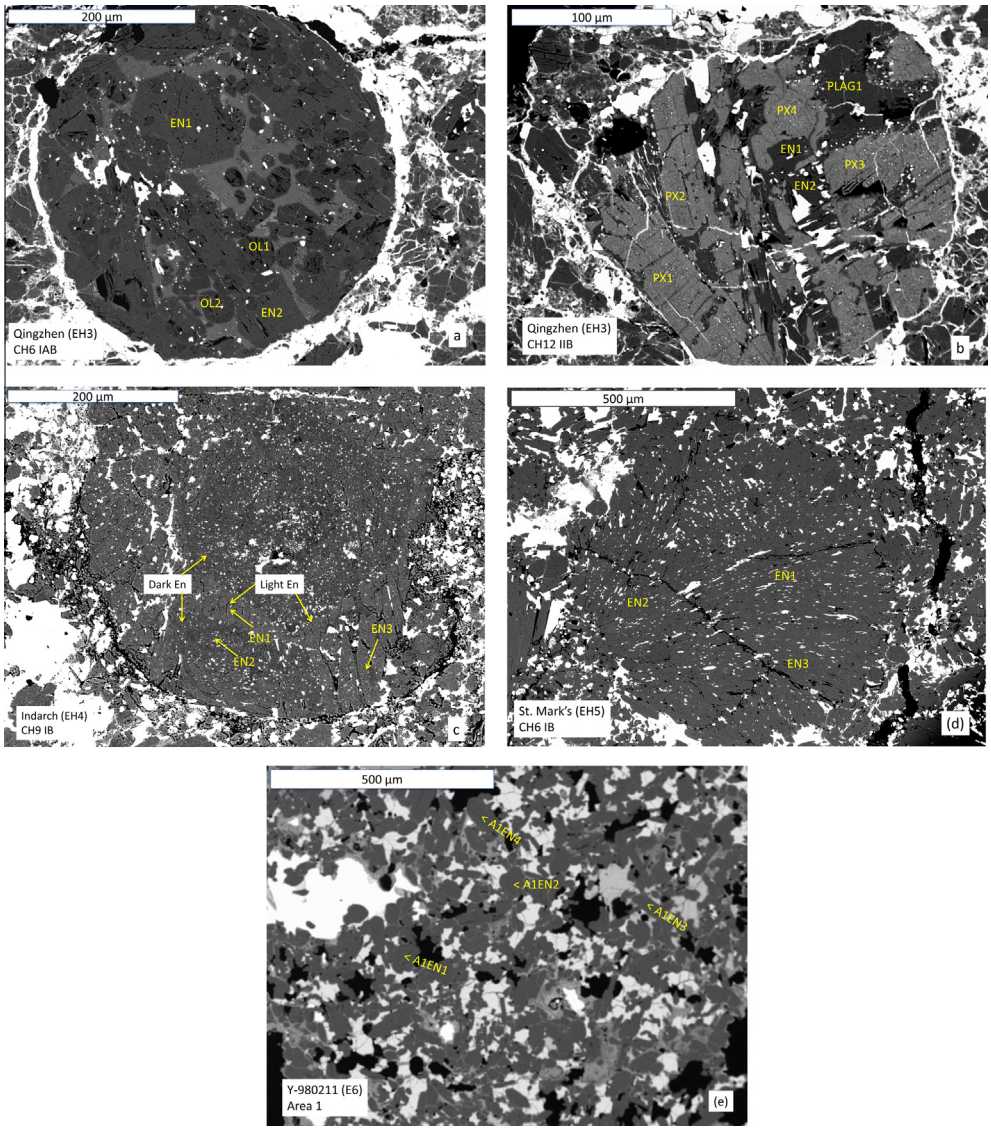

Fig. 3. Backscattered electron images of analyzed chondrules in EH chondrites. (a) A relatively olivine-rich porphyritic type IAB chondrule in Qingzhen (EH3). (b) An unusual chondrule in Qingzhen, with both enstatite and FeO-rich pyroxene (PX). This chondrule was also described by Lusby et al. (1987). (c) A coarse-grained chondrule in Indarch (EH4) with both minor element-rich (light) and minor element-poor (dark) enstatite. (d) A type IB chondrule in St. Mark's (EH5). (e) A representative area in Y-980211 (EH6). PLAG: plagioclase; other abbreviations as in Fig. 1.

3.1.3. LL chondrites

With one exception (LAR 06674, LL3.8), the members of this suite (Table 1) are falls. Images of a chondrule from each sample are shown in Fig. 2. From three to six chondrules were analyzed in each of the types 3–5 samples plus spots in two areas of St. Severin. A total of 32 chondrules were analyzed. Both type I and type II chondrules were analyzed in each unequilibrated sample, so a wide range of FeO contents was encountered. Contents of TiO_2 range from below detection to 0.10 wt% in olivine and from below detection to 0.38 wt% in pyroxene.

3.1.4. E chondrites

Suites of EH and EL chondrites were analyzed. Except for an anomalous chondrule (CH12) in Qingzhen (Fig. 3b) that has pyroxene with 14–16 wt% FeO, E-chondrite pyroxene analyzed for this study has <4 wt% FeO, and most has <1 wt%. Most TiO_2 contents are <0.15 wt%. Olivine-bearing chondrules are mainly found in type 3 (unequilibrated) E chondrites. They are rare in type 4 samples and are not found in higher-grade E chondrites. Backscattered electron images of the EH chondrites considered here are shown in Fig. 3.

Leitch and Smith (1980, 1982) and Weisberg et al. (1994), on the basis of cathodoluminescence properties, recognized different types of enstatite in unequilibrated enstatite chondrites. These workers identified blue- and red-luminescing pyroxene and found that the latter have higher TiO_2, Al_2O_3, Cr_2O_3, MnO and CaO and lower Na_2O contents than the former. The minor element-rich

Table 2
Representative electron probe analyses of minor element-rich (MER) and minor element-poor (MEP) enstatite in the E chondrites Qingzhen (QZ) and Indarch (IND).

	QZ MER	QZ MEP	IND MER	IND MEP
Na_2O	BDL	0.16	BDL	0.06
MgO	39.77	39.90	39.34	40.42
Al_2O_3	0.33	0.29	0.65	0.05
SiO_2	58.96	60.04	59.10	59.82
CaO	0.20	0.03	0.34	0.03
TiO_2	0.05	BDL	0.10	BDL
Cr_2O_3	0.39	0.04	0.36	BDL
MnO	0.11	BDL	0.09	BDL
FeO	0.77	0.29	0.54	0.06
Total	100.61	100.75	100.52	100.44
Na	0.001	0.010	0	0.004
Si	1.973	1.997	1.976	1.993
Mg	1.984	1.978	1.960	2.007
Al	0.013	0.011	0.026	0.002
Ca	0.007	0.001	0.012	0.001
Ti	0.001	0	0.003	0
Cr	0.010	0.001	0.009	0
Mn	0.003	0.001	0.003	0
Fe	0.022	0.008	0.015	0.002
Total	4.015	4.007	4.004	4.009

BDL = below detection limit of 0.02 wt% Na_2O or 0.03 wt% TiO_2, Cr_2O_3, or MnO.

pyroxene can also be recognized by its relatively higher electron albedo (brightness) in backscattered electron images (e.g., Fig. 3c). Representative electron probe analyses of minor element-rich and minor element-poor enstatite are given in Table 2.

3.1.5. Ti valence and FeO content

The valence of Ti in olivine in the ordinary chondrites is plotted against fayalite (Fa) content in Fig. 4. The most reduced Ti is found in a type I chondrule in Semarkona (LL3.0) first described by Simon et al. (2008). Except for the Semarkona data (Fig. 4c), the valence of Ti shows no correlation with Fa; the valence in most spots is $\geqslant 3.6$ regardless of Fa content. While many analyses are within error of 4.0, note that Fig. 4 shows analyses of FeO-bearing olivine, from all grades, in which 10–40% of the Ti is trivalent (i.e., valence ranges from 3.9 to 3.6, respectively). It is also clear that while the ranges of Fa content are narrower in the equilibrated samples than in the unequilibrated samples, the ranges of Ti valence observed in the grades 5 and 6 samples are not narrower than in the unequilibrated samples. Our suite of analyses of olivine in enstatite chondrites is limited due to the rarity of the phase and an analytical problem: analyses of olivine in MAC 02747 (EL4) were attempted but did not yield useful XANES spectra due to peak broadening encountered in this sample. This effect caused excessive overlap between the pre-edge peak and the absorption edge, preventing reliable extraction of the pre-edge structure. Four analyses of olivine in Qingzhen (EH3) were obtained, yielding Ti valences of 3.73 ± 0.07, 3.78 ± 0.07, 3.40 ± 0.07, and 3.71 ± 0.07, and one from PCA 91020 (EL3), 3.36 ± 0.05, were obtained. These results are typical chondritic values.

The valence of Ti in pyroxene in the ordinary chondrites is plotted against ferrosilite (Fs) content in Fig. 5. Pyroxenes with Ti valences within 1σ of 4 are rarer in the L and LL chondrites than in the H chondrites. As was found for olivine, the most reduced Ti is found in FeO-poor grains in LL chondrites, but otherwise no general trend of either increasing or decreasing valence with Fs is observed. Also as in olivine, trivalent Ti was found in most spots, and ranges of valence do not decrease with increasing petrologic type.

The valence of Ti in pyroxene in the enstatite chondrites is plotted against Fs content in Fig. 6. Valences are generally lower than in the ordinary chondrites, with very few analyses approaching 4.0 and most values between 3.2 and 3.8 in the EH chondrites, and most values below 3.6 in the EL chondrites. Thus, as in the ordinary chondrites, both Ti^{3+} and Ti^{4+} are present in most cases. In the E chondrites, Ti^{3+} dominates, unlike the ordinary chondrites, in which Ti^{4+} dominates. Also unlike the ordinary chondrites,

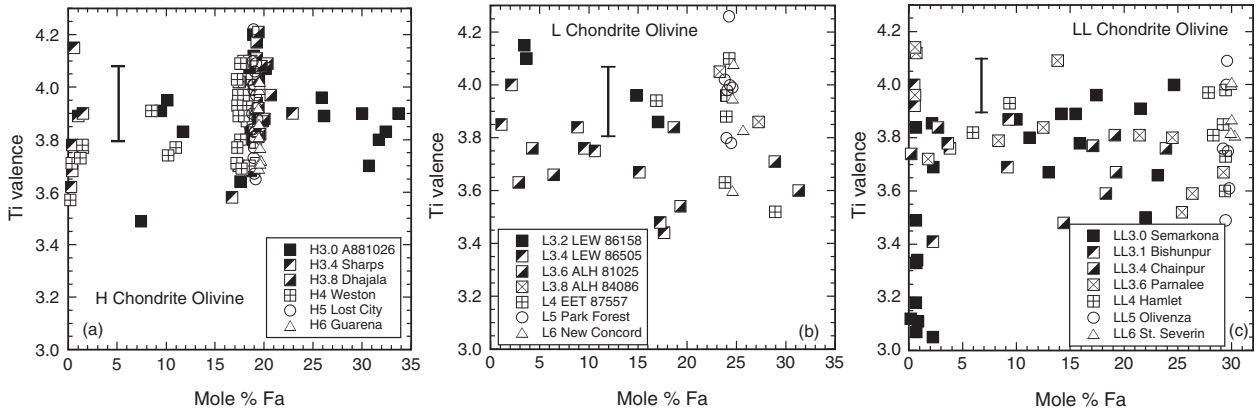

Fig. 4. Valence of Ti in olivine in ordinary chondrites plotted against fayalite (Fa) content. Data points are individual spot analyses. Error bars represent average 1σ uncertainties and show the ranges of analyses that are within 1σ of 4.0. (a) H chondrites. Error bar = $\pm$ 0.12. (b) L chondrites. Error bar = $\pm$ 0.11. (c) LL chondrites. Error bar = $\pm$ 0.10.

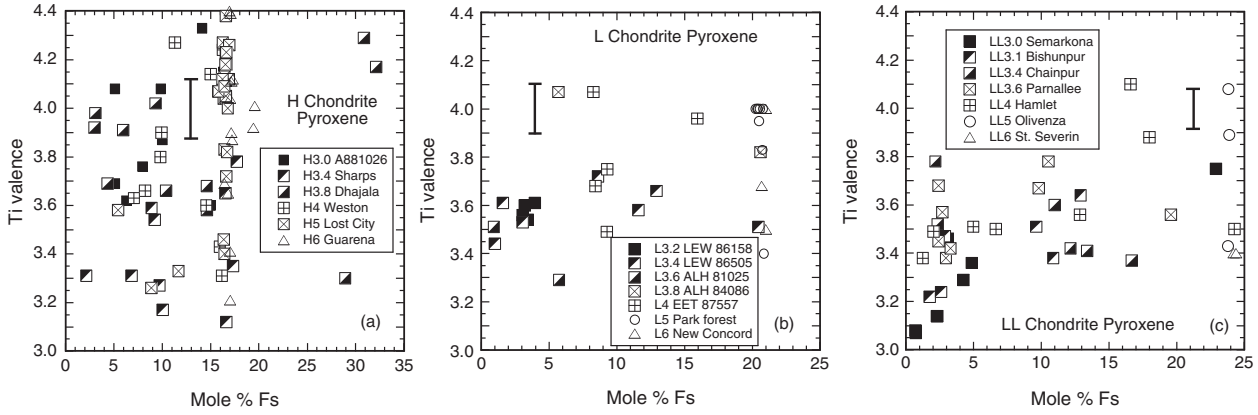

Fig. 5. Valence of Ti in pyroxene in ordinary chondrites plotted against ferrosilite (Fs) content. Data points are individual spot analyses. Error bars represent average 1σ uncertainties and show the ranges of analyses that are within 1σ of 4.0. (a) H chondrites. Error bar = ±0.12. (b) L chondrites. Error bar = ±0.10. (c) LL chondrites. Error bar = ±0.08.

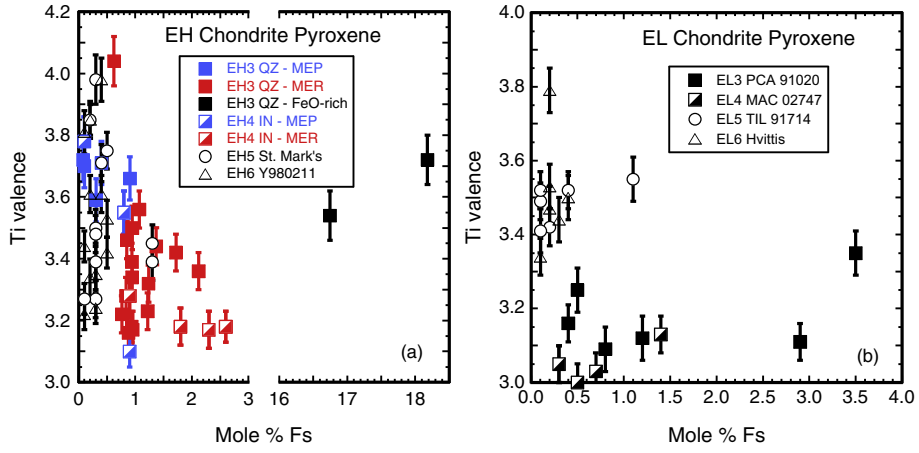

Fig. 6. Valence of Ti in pyroxene in enstatite chondrites plotted against ferrosilite (Fs) content. Data points are individual spot analyses. Error bars on valences are 1σ. (a) EH chondrites. (b) EL chondrites.

in the E chondrites the range of valence increases, tending to extend to higher values, with decreasing Fs content. Note the wide ranges of the valences in the St. Mark's (EH5) and Y980211 (EH6) analyses. The valence of Ti in the FeO-rich pyroxene in Qingzhen is well within the range of the other analyses, not near 4 as might be expected. As shown in Fig. 6a, the minor element-rich pyroxene in Qingzhen and Indarch tends to have higher Fs contents (1–3 mol%) and more reduced Ti (mostly 3.15–3.55) relative to the minor element-poor pyroxene (<1, mostly 3.55–3.8) in those meteorites.

3.1.6. Ti valence and petrologic type

The valence and coordination of Ti in olivine and pyroxene in the four groups of chondrites studied are summarized in Figs. 7 and 8. The data points, one per meteorite, are averages of average valences of each chondrule analyzed in each sample. Chondrule averages for a given phase were obtained by merging the spectra for that phase that were collected from the same chondrule. The error bars are the standard errors on sample averages. This treatment mitigates orientation effects, reveals trends that are obscured by the scatter of the individual analyses (Figs. 4–6), and allows comparison of the trends by group and comparison of olivine (left) and pyroxene (right) in the same group. The complete set of averages and standard errors is given in Table 3.

Olivine with the most reduced Ti is found in type 3.0 LL and E chondrites. Olivine in the other very low-grade samples has average valences >3.6. Among the LLs, Ti valence increases from type 3.0 (Semarkona) to 3.15 (Bishunpur) and, as in the other ordinary chondrites, valence decreases and then increases with increasing type from 3.2 to 3.8, and decreases slightly from type 3.8 to 4. The trends in the types 4 to 6 ordinary chondrites differ: H chondrite valence is flat; L valences increase then decrease slightly; and LL valences are flat at ~3.8 in types 4 and 5 and increase to 3.96 in type 6. Among the E chondrites, olivine was found only in the type 3 samples.

Valences of Ti in pyroxene also increase sharply in the ordinary chondrites (Fig. 7) between types ~3.4 and 4 and level off in the higher types, but at different values: ~3.95 in the Hs, and 3.65 in the LLs. In the Ls, the types

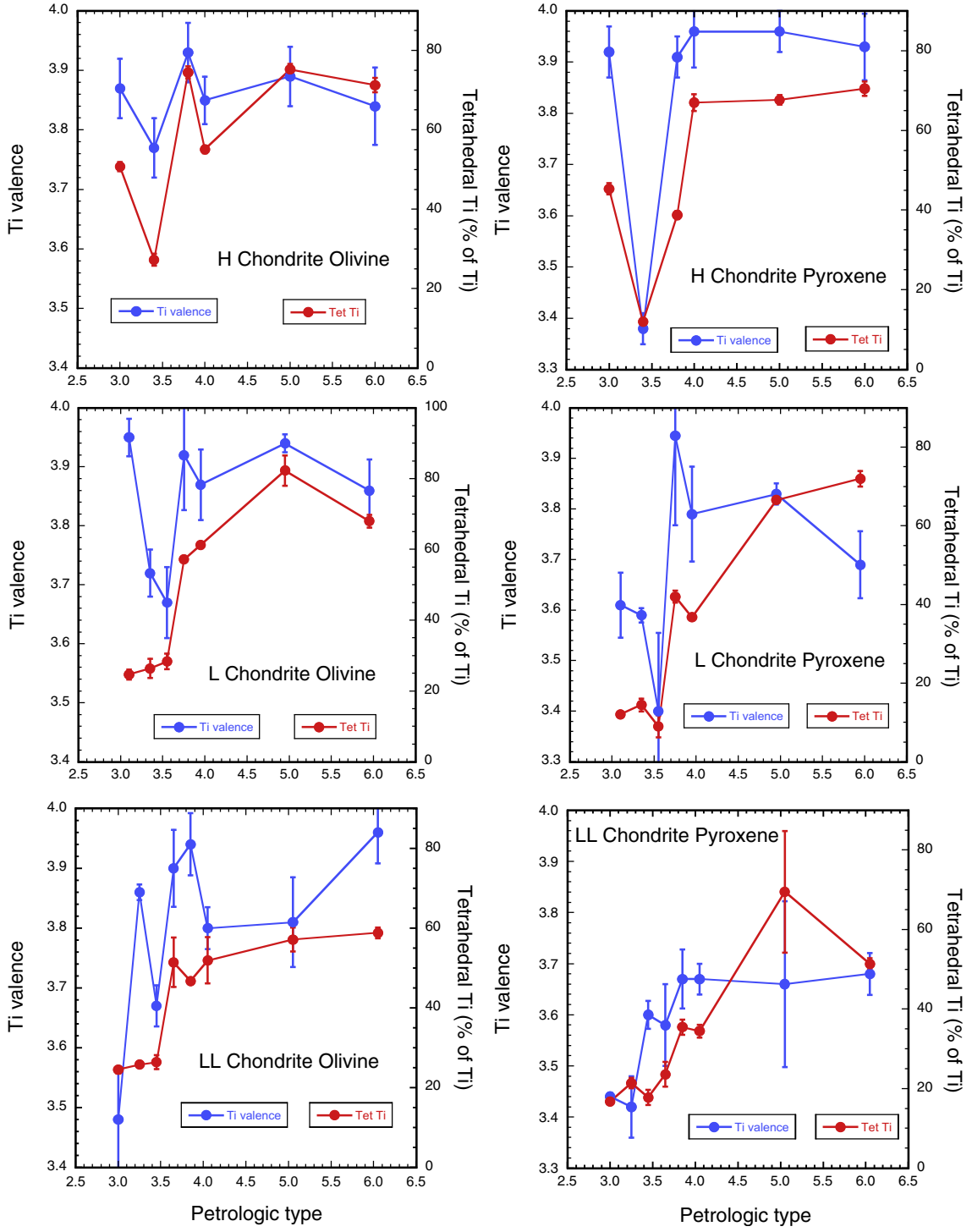

Fig. 7. Valence of Ti and proportions of Ti in tetrahedral coordination in ordinary chondrites as a function of petrologic type. Data points are averages of chondrule averages for each meteorite. Error bars represent the standard errors on these averages. Note sharp increases in Ti valence and tetrahedral Ti proportions in all suites.

4 and 5 samples average 3.8, slightly higher than the average of 3.7 found for the type 6 sample. Among the EH chondrites (Fig. 8), the average Ti valence is ~3.4 in the type 3 to 4 samples and ~3.55 in types 5 and 6. In both the EH and EL chondrites, average valence is lower in types 3 and 4 than in types 5 and 6. Ti in the types 3 and 4 EL chondrites is more strongly reduced than that in the EH chondrites. In pyroxene, Ti is mostly trivalent in the enstatite chondrites and mostly tetravalent in most of the ordinary chondrites.

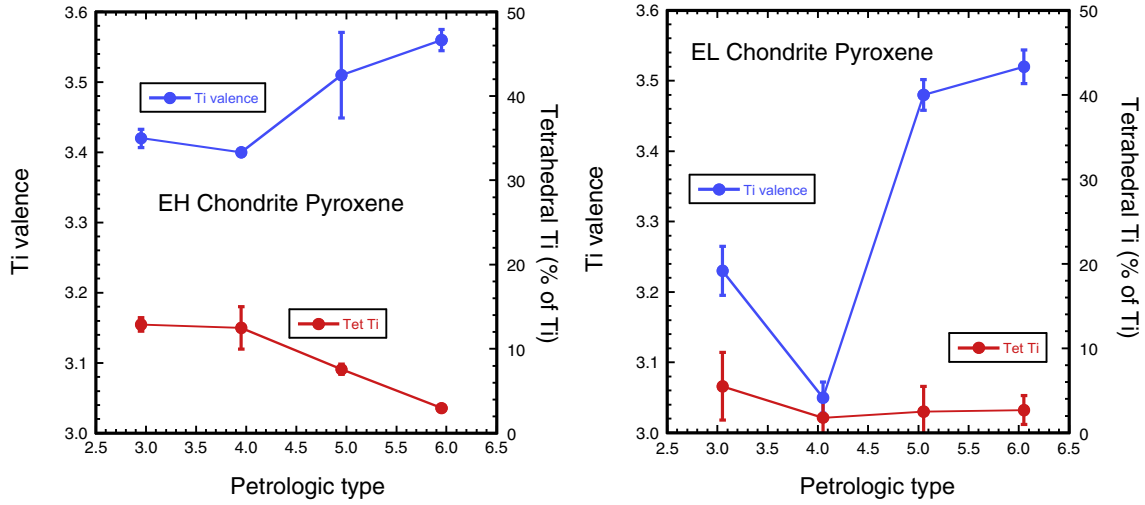

Fig. 8. Valence of Ti and proportions of Ti in tetrahedral coordination in enstatite chondrites as a function of petrologic type. Data points are averages of chondrule averages for each sample. Error bars represent the standard errors on these averages. Note the contrast with the trends seen in the analogous data for ordinary chondrites.

3.1.7. Ti coordination and petrologic type

The average percentages of Ti in tetrahedral coordination in olivine and pyroxene are also illustrated in Figs. 7 and 8. In general, both phases tend to have lower tetrahedral Ti^{4+} proportions in the low-grade ordinary chondrites than in the higher-grade ($\geqslant$3.8) samples. The coordination environments of Ti in olivine and pyroxene in the L and LL chondrites exhibit similar variations with type: low tetrahedral Ti contents in the low-grade (<3.6) samples; sharp increases between the lowest-grade samples and type 3.6 or 3.8 samples; slight or no decreases to type 4; increases to type 5 or 6. Olivine and pyroxene in the H3.0 (A-881026) sample have higher tetrahedral Ti proportions than the other low-grade OCs, but like the latter, the H chondrites also show sharp increases in tetrahedral Ti between types 3.4 and 3.8.

In contrast with the ordinary chondrites, the enstatite chondrites do not exhibit sharp increases in tetrahedral Ti proportions with grade. The type 3 E chondrites have tetrahedral Ti proportions similar to those of the low-grade ordinary chondrites. In the EH chondrites, tetrahedral Ti proportions decrease with increasing grade, and in the EL chondrites the proportions are low at all grades; both trends strongly differ from the trends (sharp increases with petrologic type) seen in the ordinary chondrite data.

4. DISCUSSION

4.1. Valence of Ti in chondrites

Interchondrule variations in Ti valence are seen in all equilibrated and unequilibrated ordinary and enstatite chondrites, and the standard deviations do not systematically decrease with increasing grade. The use of merged spectra makes it very unlikely that this observation is due to orientation effects. The observation of ranges of Ti^{3+}/Ti^{4+} ratios in FeO-bearing silicates also indicates that the valence of Ti did not equilibrate to the same extent as that of Fe. The data do suggest, however, that metamorphism did affect the valence of Ti. It is generally more reduced in the unequilibrated OCs than in the equilibrated OCs. As Fig. 7 shows, the valence of Ti in olivine and pyroxene, on average, decreases and increases with increases in type from 3 to 4 (except for pyroxene in the LLs, which does not show a decrease), and it remains relatively high through the high grades. Among the ordinary chondrites, however, the type 3.6 to 4 samples tend to have higher valences than the lower-grade samples. This suggests that oxidation occurred below type 4, whereas redox indicators based on Fe are consistent with reduction between types 3 and 4 and oxidation at higher grades (Menzies et al., 2005). In both groups of enstatite chondrites, the types 5 and 6 samples are oxidized relative to the lower-grade ones (Fig. 8), but overall the Ti in the E chondrites is very reduced compared to that in the ordinary chondrites.

The resistance of Ti to redox equilibration at conditions where Fe redox state and Fe/Mg ratios did equilibrate could account for the coexistence of trivalent Ti with oxidized Fe, in a scenario in which chondrule precursors were formed under reducing conditions, records of which are retained in the valence of Ti in olivine and pyroxene (e.g., Simon et al., 2008). During melting of chondrule precursors and crystallization under relatively oxidizing conditions, metallic Fe oxidized and entered silicate phases while trivalent Ti was retained, even in type II chondrules. Preliminary results of dynamic crystallization experiments on chondrule-composition melts (Simon et al., 2011, 2014) indicate that, in charges initially equilibrated at relatively reducing (IW-3) conditions, Fe does indeed oxidize more readily than Ti during cooling under relatively oxidizing (IW-0.5) conditions.

Formation of the phases in enstatite chondrites, such as pure enstatite, Si-bearing metal, and Mg-sulfides, requires a lower fO_2 than can be generated from a system of solar composition, usually considered to result from a system with C/O greater than the solar value of 0.5 (Grossman

Table 3
Average valences of Ti and proportions of Ti in tetrahedral coordination in olivine and pyroxene in ordinary and enstatite chondrites.

Sample	Ol val.[a]	Ol S.E.[b]	Ol ^{IV}Ti[c]	^{IV}Ti S.E.[d]	Px val.[a]	Px S.E.[b]	Px ^{IV}Ti[c]	^{IV}Ti S.E.[d]
H chondrites								
A-881026	3.87	0.05	50.8	1.2	3.92	0.05	45.4	1.4
Sharps	3.77	0.05	27.3	1.5	3.38	0.03	12.0	0.5
Dhajala	3.93	0.05	74.5	1.5	3.91	0.04	38.8	1.0
Weston	3.85	0.04	55.1	1.0	3.96	0.07	67.0	2.1
Lost City	3.89	0.05	75.3	1.4	3.96	0.04	67.7	1.2
Guareña	3.84	0.07	71.3	1.8	3.93	0.07	70.5	1.8
L chondrites								
LEW 86158	3.95	0.03	24.7	1.4	3.61	0.06	12.1	0.6
LEW 86505	3.72	0.04	26.4	2.7	3.59	0.01	14.5	1.6
ALHA 81025	3.67	0.06	28.4	2.2	3.40	0.16	9.0	2.8
ALH 84086	3.92	0.09	57.2	0.8	3.94	0.18	42.0	1.5
EET 87557	3.87	0.06	61.3	0.8	3.79	0.09	36.8	0.7
Park Forest	3.94	0.02	82.3	4.3	3.83	0.02	66.6	0.6
New Concord	3.86	0.05	68.0	1.8	3.69	0.07	72.0	2.0
LL chondrites								
Semarkona	3.48	0.08	24.5	0.9	3.44	0.01	16.8	0.3
Bishunpur	3.86	0.01	25.8	0.6	3.42	0.06	21.4	1.3
Chainpur	3.67	0.03	26.4	1.7	3.60	0.03	17.8	1.9
Parnallee	3.90	0.06	51.4	6.2	3.58	0.08	23.6	3.1
LAR 06674	3.94	0.05	46.7	0.7	3.67	0.06	35.5	1.9
Hamlet	3.80	0.04	51.9	5.8	3.67	0.03	34.5	1.6
Olivenza	3.81	0.08	57.1	3.0	3.66	0.16	69.5	15.3
St. Severin	3.96	0.05	58.8	1.3	3.68	0.04	51.4	1.4
EH chondrites								
Qingzhen	3.66	0.17	17.3	0.6	3.42	0.01	12.9	0.8
Indarch	–	–	–	–	3.40	0.01	12.5	2.5
St. Mark's	–	–	–	–	3.51	0.06	7.6	0.6
Y-980211	–	–	–	–	3.56	0.02	3.0	0.3
EL chondrites								
PCA 91020	3.36	0.05	2	–	3.23	0.04	5.5	4.0
MAC 02747	–	–	–	–	3.05	0.02	1.8	2.5
TIL 91714	–	–	–	–	3.48	0.02	2.5	3.0
Hvittis	–	–	–	–	3.52	0.02	2.7	1.7

[a] Average Ti valence in olivine (OL) or pyroxene (Px) calculated from chondrule averages for each sample.
[b] Standard error (S.E.) for the olivine or pyroxene average valence.
[c] Percentage of Ti that is in tetrahedral coordination in olivine (Ol) or pyroxene (Px).
[d] Standard error (S.E.) for the olivine or pyroxene average tetrahedral Ti proportion.

et al., 2008). This leads to the reasonable expectation that all Ti in E chondrites is trivalent, but this is not observed. Instead, Ti^{4+} is found in all pyroxene and olivine analyzed in the E chondrites (Fig. 6), supporting previous suggestions that E chondrites formed from oxidized precursors that underwent reduction (Lusby et al., 1987; Weisberg et al., 1994). The average Ti valence in the most equilibrated of the enstatite chondrites is ~3.4 to 3.5. If these valences represent at least an approach to equilibrium, the subequal Ti^{3+}/Ti^{4+} ratios (proportions of Ti^{3+} and Ti^{4+}) more likely represent near-solar conditions rather than a system lower in fO_2 by several orders of magnitude. Solar fO_2s, 6–8 orders of magnitude below the IW buffer, are also indicated by the model of Lehner et al. (2013) for the silicate sulfidation of enstatite chondrites. As noted by Grossman et al. (2008), removal of high-temperature condensates from a system whose composition is solar except for a C/O ratio of 0.83 can yield condensates whose major element bulk composition is that of enstatite chondrites. In addition, the condensates are predicted to have high enstatite:forsterite ratios and several wt% Si in coexisting nickel–iron, as observed in E chondrites. Such a system would have an fO_2 ~2.1 log units below that of a nominal system of solar composition (Grossman et al., 2008), possibly accounting for the presence of Ti^{4+} in E-chondrite silicates, as this is just 0.5 log unit below the average fO_2 derived experimentally for Allende refractory inclusions (Grossman et al., 2008).

The difference in valence between minor element-rich (MER) and minor element-poor (MEP) enstatite (Fig. 6a) supports previous suggestions (Leitch and Smith, 1982; Weisberg et al., 1994) that they represent different generations of materials and that redox conditions varied within the enstatite chondrite formation region. In the context of the model of Weisberg et al. (1994), in which MER enstatite formed by solid-state reduction of relatively

FeO-rich, non-luminescing pyroxene followed by condensation of MEP enstatite, the present data imply that the reduction step occurred at a lower fO_2 than the condensation step and was of sufficient duration to allow significant reduction of both Fe and Ti, but not full equilibration of the latter. The MEP enstatite may have formed under slightly more oxidizing conditions than those to which the MER was exposed, and with lower proportions of minor elements available than when the earlier pyroxene formed, leading to its purer, near-endmember compositions.

4.2. Valence of Ti and Substitution into olivine and pyroxene

In both of these nominally Ti-free phases, Ti^{3+} can enter octahedrally coordinated cation sites and Ti^{4+} can enter tetrahedral and octahedral sites. When Ti enters an octahedral site in these phases, it is typically replacing a divalent cation, creating a charge excess of either +1 (Ti^{3+}) or +2 (Ti^{4+}). This requires coupled substitution, typically with Al^{3+} replacing Si^{4+} in a tetrahedral site, in order to maintain charge balance; two Al cations must replace two Si cations for each Ti^{4+}. The Ti-Al coupled substitution is such an important mechanism that lunar pyroxenes with atomic Ti/Al ratios >0.5 have long been inferred to contain Ti^{3+} (e.g., Weill et al., 1971; Papike, 1998). If little or no Al or Fe^{3+} are available, however, substitution of Ti^{4+} for Si^{4+} in the tetrahedral site may occur (Sepp and Kunzmann, 2001). This direct substitution has been shown to be energetically favored over other substitutions in olivine under anhydrous conditions (Berry et al., 2007). If H is available in the absence of Al, charge compensation for Ti substitution into octahedral sites can be accomplished by formation of OH^- groups coordinated around Si site vacancies, a configuration known as Ti-clinohumite-like defects (Berry et al., 2007). In this case, substitution of Ti^{4+} for a divalent cation (+2 excess) is compensated by a tetrahedral site vacancy (−4 deficit) coordinated by two oxygen anions and two hydroxyl groups (+2 compared to coordination by four oxygen anions). The extent to which Ti has substituted into tetrahedral vs. octahedral sites in olivine and pyroxene thus may be an indicator of the chemical environment(s) under which it entered those phases.

4.3. Variation of proportions of tetrahedrally coordinated Ti with petrologic type: The effect of valence changes

All suites of ordinary chondrites exhibit sharp increases in tetrahedral Ti proportions between type 3.5 and type 4 samples, and in all cases except in LL pyroxene, these increases accompany increases in average valence (Fig. 7). In the enstatite chondrites (Fig. 8), Ti is more oxidized in the types 5 and 6 samples than in the types 3 and 4 samples as well, but here the higher valences are not accompanied by higher proportions of tetrahedral Ti. In the ordinary chondrites, valence and tetrahedral Ti proportions are directly correlated in both olivine and pyroxene despite their different substitution mechanisms for Ti, but these parameters are anticorrelated in the EH chondrites and uncorrelated in the ELs. The present results show that pyroxene and olivine in the ordinary chondrites responded to metamorphism in a similar manner, but one that was different from the response of pyroxene in the enstatite chondrites.

The present results support the previous inferences from a variety of observations and measurements that low-grade ordinary chondrite metamorphism occurred under relatively reducing conditions; higher-grade environments were relatively oxidizing; and types 4–6 H chondrites record uniform redox conditions. If the trends shown in Fig. 7 reflect responses to metamorphism, then the change from reducing to oxidizing conditions was rather abrupt, as might be expected for a change in the nature of the dominant equilibria, such as from carbon-dominated to aqueous fluid-dominated. It has been suggested that reduction of Fe by graphite was important during the metamorphism of ordinary chondrites from type 3 toward 4 (McSween and Labotka, 1993) and that oxidation occurred during metamorphism from type 4 through 6 due to the presence of water derived from the melting of ice that had accreted onto the parent bodies prior to metamorphism (McSween and Labotka, 1993). The results shown in Fig. 7 are consistent with this sequence. There is evidence, however, for limited hydration in very low-grade chondrites. For example, smectite is present in the matrix of Semarkona (Hutchison et al., 1987). Thus, although water may have been present throughout chondrite metamorphism, reduction, presumably by carbon, was dominant in the early stages/low grades. All suites show some reduction between types 3 and ~3.5 and most show sharp increases in the valence of Ti between types 3.5 and 4 (Fig. 7); it has been shown that carbon contents of unequilibrated chondrites decrease with increasing grade from type 3 to 4, reaching zero at about type 4 (Menzies et al., 2005). Thus, the sharp Ti valence increases observed in the present work occur at the stage where the presumed reducing agent is exhausted.

In contrast, the enstatite chondrites are thought to have never been hydrated, with parent bodies that did not accrete ice, and they exhibit quite different valence/coordination trends with grade from the ordinary chondrites. This is to be expected if the presence of water was necessary for the oxidation of Ti^{3+} to Ti^{4+} seen in the ordinary chondrite data. In the EL chondrites, although valence increases slightly from grades 4 through 6, the proportions of tetrahedral Ti decrease slightly, and all of the EL samples have very low tetrahedral Ti contents, also unlike the ordinary chondrites, in which these parameters are positively correlated.

If Ti were incorporated into chondrule olivine by the defect mechanism described above, then the increases in tetrahedral Ti proportions could be due to loss of H during heating, breakdown of hydroxyl groups and filling of tetrahedral vacancies by nearby Ti cations that had been in octahedral sites. This was suggested by Simon et al. (2012) but may not be the best explanation. Pyroxene also shows sharp increases in tetrahedral Ti proportions, but the defect mechanism has not been inferred for the substitution of Ti into pyroxene, so loss of H during heating is not likely to account for high tetrahedral Ti contents in pyroxene. The similar responses to metamorphism indicated by the nearly identical valence and coordination trends with grade in

olivine and pyroxene in the ordinary chondrites suggest that similar processes affected both phases. The correlation between valence and tetrahedral Ti proportions suggests that the increases in the latter are likely due to the increases in total Ti^{4+} caused by oxidation during metamorphism.

5. SUMMARY AND CONCLUSIONS

Whereas the FeO/MgO ratios of ferromagnesian silicates in the ordinary chondrites are equilibrated by type 4, ranges of Ti valences in these samples do not decrease with increasing grade. It is clear that the valence of Ti does not equilibrate as readily as that of Fe. This characteristic can account for the occurrence of trivalent Ti in FeO-bearing silicates. The valence of Ti in ordinary chondrites may have partially responded to the redox environment during metamorphism, however. On average, it tends to be more reduced in unequilibrated ordinary chondrites than in samples of types 4–6, and valence increases in olivine and pyroxene in all ordinary chondrites between types 3.5 and 4, approximately the stage at which it is thought that carbon was exhausted and therefore lost as a reducing agent. In enstatite chondrites, Ti^{4+} was found in all samples but overall Ti is more reduced than in the ordinary chondrites, and the EH and EL chondrites exhibit different coordination-grade relationships from each other and from the ordinary chondrites. This implies that the enstatite and ordinary chondrites were exposed to different redox environments during metamorphism on their parent bodies.

ACKNOWLEDGMENTS

We thank ANSMET, the Field Museum of Natural History, the National Institute of Polar Research (Japan), the National Museum of Natural History (US) and the University of New Mexico for loans of samples. Comments by AE S. Russell, reviewer J. Karner and two anonymous reviewers led to improvements in the text. Portions of this work were conducted at GeoSoilEnviroCARS (Sector 13), Advanced Photon Source (APS), Argonne National Laboratory. GeoSoilEnviroCARS is supported by NSF (EAR-1128799) and DOE-Geosciences (DE-FG02-94-ER14466). Other portions of this work were supported by NASA through grants NNX13AE73G (L. Grossman, PI) and NNX16AI26G (S. Simon, PI). All funding is gratefully acknowledged.

REFERENCES

Berry A. J., Walker A. M., Hermann J., O'Neill H., St C., Foran G. J. and Gale J. D. (2007) Titanium substitution mechanisms in forsterite. *Chem. Geol.* **242**, 176–186.

Brearley A. J. and Jones R. H. (1998) Chondritic meteorites. In *Planetary Materials* (ed. J. J. Papike). *Revs. Mineralogy* **36**, 3-1–3-398.

Dunn T. L., McSween H. Y., McCoy T. J. and Cressey G. (2010) Analysis of ordinary chondrites using powder X-ray diffraction: 2. Applications to ordinary chondrite parent-body processes. *Meteoritics Planet. Sci.* **45**, 135–156.

Gastineau-Lyons H. K., McSween H. Y. and Gaffey M. J. (2002) A critical evaluation of oxidation versus reduction during metamorphism of L and LL group chondrites, and implications for asteroid spectroscopy. *Meteoritics Planet. Sci.* **37**, 75–89.

Grossman L., Beckett J. R., Fedkin A. V., Simon S. B. and Ciesla F. J. (2008) Redox conditions in the solar nebula: Observational, experimental, and theoretical constraints. In *Oxygen in the Solar System* (eds. G. J. MacPherson, D. W. Mittlefehldt, J. H. Jones and S. B. Simon). *Revs. Mineral. Geochem.* **68**, 93–140.

Huss G. and Lewis R. S. (1995) Presolar diamond, SiC, and graphite in primitive chondrites: abundances as a function of meteorite class and petrologic type. *Geochim. Cosmochim. Acta* **59**, 115–160.

Hutchison R., Alexander C. M. O. and Barber D. J. (1987) The Semarkona meteorite: first recorded occurrence of smectite in an ordinary chondrite, and its implications. *Geochim. Cosmochim. Acta* **51**, 1875–1882.

Kessel R., Beckett J. R. and Stolper E. M. (2007) The thermal history of equilibrated ordinary chondrites and the relationship between textural maturity and temperature. *Geochim. Cosmochim. Acta* **71**, 1855–1881.

Lehner S. W., Petaev M. I., Zolotov M. Yu. and Buseck P. R. (2013) Formation of niningerite by silicate sulfidation in EH3 enstatite chondrites. *Geochim. Cosmochim. Acta* **101**, 34–56.

Leitch C. A. and Smith J. V. (1980) Two types of clinoenstatite in the Indarch enstatite chondrite. *Nature* **283**, 60–63.

Leitch C. A. and Smith J. V. (1982) Petrography, mineral chemistry and origin of Type I enstatite chondrites. *Geochim. Cosmochim. Acta* **46**, 2083–2097.

Lusby D., Scott E. R. D. and Keil K. (1987) Ubiquitous high-FeO silicates in enstatite chondrites. *Proc. Lunar Planet. Sci. Conf. 17th J. G. R.* **92**, E679–E695.

McSween H. Y. and Labotka T. C. (1993) Oxidation during metamorphism of the ordinary chondrites. *Geochim. Cosmochim. Acta* **57**, 1105–1114.

Menzies O. N., Bland P. A., Berry F. J. and Cressey G. (2005) A Mössbauer spectroscopy and X-ray diffraction study of ordinary chondrites: quantification of modal mineralogy and implications for redox conditions during metamorphism. *Meteoritics Planet. Sci.* **40**, 1023–1042.

Papike J. J. (1998) Comparative planetary mineralogy: Chemistry of melt-derived pyroxene, feldspar, and olivine. In *Planetary materials* (ed. J.J. Papike). *Revs. in Mineralogy* **36**, 7-1–7-11.

Pouchou J. L. and Pichoir F. (1984) A new model for quantitative X-ray microanalysis. Part I: application to the analysis of homogeneous samples. *Rech. Aerosp.* **3**, 13–38.

Quirico E., Bourot-denise M., Robin C., Montagnac G. and Beck P. (2011) A reappraisal of the metamorphic history of EH3 and EL3 enstatite chondrites. *Geochim. Cosmochim. Acta* **75**, 3088–3102.

Rubin A. E. and Wasson J. T. (2011) Shock effects in "EH6" enstatite chondrites and implications for collisional heating of the EH and EL parent asteroids. *Geochim. Cosmochim. Acta* **75**, 3757–3780.

Sepp B. and Kunzmann T. (2001) The stability of clinopyroxene in the system CaO–MgO–SiO_2–TiO_2 (CMST). *Am. Mineral.* **86**, 265–270.

Simon S. B., Sutton S. R. and Grossman L. (2007) Valence of titanium and vanadium in pyroxene in refractory inclusion interiors and rims. *Geochim. Cosmochim. Acta* **71**, 3098–3118.

Simon S. B., Sutton S. R. and Grossman L. (2008) Constraints on the oxidation state of chondrule precursors from titanium XANES analysis of Semarkona chondrules. In *Lunar and Planet. Sci.*, XXXIX. Lunar Planet. Inst., Houston, #1352 (abstr.).

Simon S. B., Beckett J. R., Vaughan W. M., Sutton S. R. and Grossman L. (2011) Chondrule-composition melts: Response of Fe and Ti valence to changing redox conditions. In *Lunar and Planet. Sci.*, XLII. Lunar Planet. Inst., Houston, #1271 (abstr.).

Simon S. B., Sutton S. R. and Grossman L. (2012) Effects of metamorphism on the valence and coordination of titanium in

ordinary chondrites. In *Papers Presented at the Forty-third Lunar and Planetary Science Conference*. Lunar and Planetary Institute, Houston. Abstract #2078.

Simon S. B., Sutton S. R. and Grossman L. (2013) The valence of Ti in enstatite chondrites: Not what you might think. In *Papers Presented at the Forty-fourth Lunar and Planetary Science Conference*. Lunar and Planetary Institute, Houston. Abstract #2270.

Simon S. B., Beckett J. R., Sutton S. R. and Grossman L. (2014) Experimental investigation of Ti and Fe valence in chondrule-like melts during cooling under changing redox conditions at low partial pressures. In *Papers presented at the 45th Lunar and Planetary Science Conference*. Abstract #1633, LPI Contribution #1777.

Simon S. B., Sutton S. R. and Grossman L. (2015) The valence and coordination of Ti in olivine and pyroxene in ordinary and enstatite chondrites as a function of metamorphic grade. In *Lunar and Planetary Science*, XLVI. Abstract #2141, LPI Contribution #1832.

Sutton S. R. and Newville M. (2014) Synchrotron X-ray spectroscopic analysis. In *Treatise on Geochemistry* (eds. K. K. Turekian and H. D. Holland), 2nd ed. Elsevier, Amsterdam, pp. 213–230.

Sutton S. R. and Rivers M. L. (1999) Hard X-ray synchrotron microprobe techniques and applications. In *Synchrotron X-ray Methods in Clay Science*, 9 (eds. D. G. Schulze, J. W. Stucki and P. M. Bertsch). CMS Workshop Lectures, pp. 146–163.

Sutton S. R., Bertsch P. M., Newville M., Rivers M., Lanzirotti A. and Eng P. (2002) Microfluorescence and microtomography analyses of heterogeneous earth and environmental materials. In *Applications of Synchrotron Radiation in Low-temperature Geochemistry & Environmental Science* (ed. P. A. Fenter et al.). Mineralogical Society of America, Chantilly, VA. *Reviews in Mineralogy & Geochemistry* **49**, 429–483.

Van Schmus W. R. and Wood J. A. (1967) A chemical-petrological classification for the chondritic meteorites. *Geochim. Cosmochim. Acta* **31**, 747–765.

Weill D. F., Grieve R. A., McCallum I. S. and Bottinga Y. (1971) Microprobe studies of samples 12021 and 12022; viscosity of melts of selected lunar compositions. In *Proc. Lunar Sci. Conf.*, 2, pp. 413–430.

Weisberg M. K., Prinz M. and Fogel M. (1994) The evolution of enstatite and chondrules in unequilibrated enstatite chondrites: evidence from iron-rich pyroxene. *Meteoritics* **29**, 362–373.

Associate editor: Sara S. Russell